Orientation Effects of Elastic-Plastic Deformation at Surfaces: Nanoindentation of Nickel Single Crystals

Oyeon Kum

Department of Chemistry, Clemson University, Clemson, SC 29634

ABSTRACT

Orientation effects in nanomechanical properties at the surfaces with molecular dyanmics were observed as a function of indenter size and indenter speed in three crystal orientations: ⟨100⟩, ⟨110⟩, and ⟨111⟩. The force vs displacement curves for indentation follows the Hertzian solution for elastic deformation of $F = kd^{1.5}$. However, the force fitted constant k showed a dependency on indenter size, velocity, and crystal orientations. The results of dislocation nucleations in different orientations also showed anisotropy: Stacking faults in the ⟨100⟩; deep partial dislocations in the ⟨110⟩; shallow partial dislocations followed by the stacking faults in the ⟨111⟩.

Keywords: nanoindentation, anisotropy, indentation curve, dislocation nucleation

1 INTRODUCTION

Large-scale simulations of single crystals, nickel, using Morse-type pair potentials, the analytical form of embedded atom method (EAM) potential, and the tabular form of the EAM potential were recently performed in bulk under shock compressed conditions [1], [2] to investigate anisotropy of fcc single crystal deformation. However, knowledge of the mechanical behavior associated with the contact of small volumes under the surface is also important from both scientific and technological viewpoints. The development of nanoindentation techniques such as interfacial force microscopy or atomic-force microscopy provide easy experimental tools to investigate the detailed mechanism of deformation during indentation at a very small scale. The results of such research contribute to the understanding of microscopic fracture mechanics to develop device miniaturization and computer disk drives.

Modern nanoindentation techniques have allowed for the measurement of load versus indentation depth curves of small volumes where the contact radius is less than 100 nm [3]. These small volumes are available sizes for large-scale molecular dynamics simulations to make direct comparisons between experiments and simulations. Such comparison may solve the discrepancies among different models and experiments. For example, a typical nanoindentation curve exhibits abrupt bursts in displacement at constant load separated by regions of positive slope, whereas a classical curve shows a relatively smooth positive slope. Such discrepancies are postulated to be driven from the discrete nucleation of dislocation loops below the indenter, but the exact mechanisms are difficult to investigate experimentally and still under discussion [4].

In this paper, I investigate the orientation effects of nickel single crystals in (100), (110), and (111) surfaces using molecular dynamics. The indenter velocity, crystal orientations, indenter sizes were important parameters for anisotropy shown in indentation curves. This study showed the atomistic insight into anomalous dislocation nucleation of single crystals at surfaces in three crystal orientations.

2 MODEL

Because a typical dislocation separation is the order of μm for well-annealed metals, the area under the nanoindenter should behave close to that of a perfect single crystal–dislocation free. In this paper, I used Voter's tabular form of embedded atom model (EAM) potential [5] to describe nickel single crystals. Previous atomistic calculations have studied indentation and retraction using EAM potentials [6], or other semiempirical potential models [7], as well as first-principles methods [8]. These calculations showed strong bonding between the indenter tip and the surface due to the large energy of adhesion between two clean surfaces. This leads to a jump to contact upon approach and necking between the tip and surface during retraction. In experiments, the tip-surface adhesion interaction will be dramatically reduced because the tip and surface are not atomically clean or surfaces are passivated by the addition of an alkanethiol layer which prevents bonding between the tip and the surface [9].

The model discussed in this work is tailored to address the passivated surfaces by using a strongly repulsive potential to describe the interactions between the indenter and the metal surfaces. Each atom in the indented material interacts with the idealized spherical indenter via the repulsive potential,

$$V(r) = \epsilon(\sigma/r)^{\alpha}, \tag{1}$$

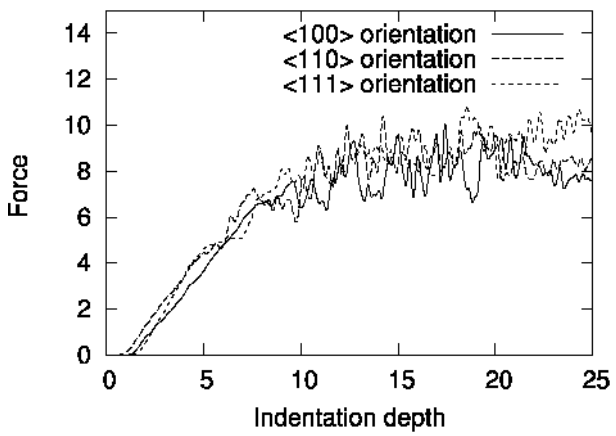

Figure 1: Indentation force vs displacement curves in the three orientations. The indenter velocity is about 670 m/sec and its diameter is 4.0 nm. Force unit is 43.59042 nN and length unit is $\mathring{A}$.

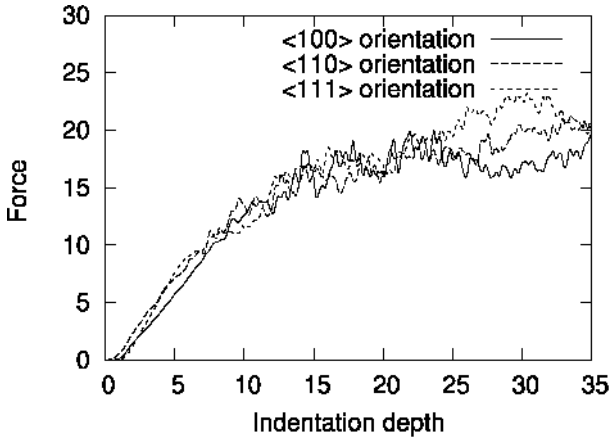

Figure 2: Indentation force vs displacement curves in the three orientation directions. The indenter velocity is about 670 m/sec and its diameter is 6.0 nm. See Fig. 1 caption for units.

where ϵ is energy, σ is the indenter radius, and r is the distance between atom and the center of the indenter. α is the power of the potential. α was chosen to be 150 in the simulations to guarantee the strong repulsive force between indenter and surface. As is customary, I used reduced (or dimensionless) quantities to specify various physical parameters. Energy unit is eV, unit of length $\mathring{A}$, and unit of mass atomic unit of nickel mass. Thus, the time unit $t_0 = (\mathrm{m}\sigma^2/\epsilon)^{1/2}$ and force unit is 43.59042 (nN).

3 RESULTS AND DISCUSSION

Simulations were performed for three indenter diameters (4.0, 5.0, and 6.0 nm) and two indenter speeds (about 670 and 67 m/sec). The indenter approaches to the cold (zero temperature) fcc nickel single crystals orientated in the $\langle 100\rangle$, $\langle 110\rangle$, and $\langle 111\rangle$ directions. The total number of atoms involved are 400 000, 397 600, and 397 440 for the $\langle 100\rangle$, $\langle 110\rangle$, and $\langle 111\rangle$ orientations, respectively.

Figure 1 shows indentation force vs displacement depth curves for three crystal orientations with indenter diameter of 4.0 nm and at the indenter velocity of about 670 m/sec. The typical features of curves for three orientations are the elastic deformations followed by the plastic deformations and all curves have displacement excursions which correspond to the initiation of plastic deformation (yield points). Overall, the indentation curves follow the Hertzian solution for elastic deformation which is a simple power law of F = k $\mathrm{d}^{1.5}$. The values of k, corresponding to indentation modulus or micro-hardness, are 0.32, 0.40, and 0.37 in the $\langle 100\rangle$, $\langle 110\rangle$, and $\langle 111\rangle$ orientations, respectively.

The force vs displacement curves for three crystal orientations with indenter diameter of 6.0 nm at the indenter velocity of about 670 m/sec are shown in Fig. 2. Larger diameter of indenter produces higher micro-hardness. The values of k are 0.45, 0.61, and 0.63 in the $\langle 100\rangle$, $\langle 110\rangle$, and $\langle 111\rangle$ orientations, respectively. The anisotropy is also shown clearly in the different orientation directions. Compared with Fig. 1, indenter size can be considered as an important parameter of anisotropy.

Figure 3 shows indentation force vs displacement curves for three orientations at the indenter velocity of about 67 m/sec with the indentor diameter of 5.0 nm. Compared with the Fig. 1 and Fig. 2, slow indenter velocity resulted in different microscopic mode of indentation curves in elastic deformation. Each orientation showed different excursion point: $\langle 110\rangle$ orientation showed the weakest yield strength and in the $\langle 100\rangle$ direction, the yield strength was the strongest. In the $\langle 111\rangle$ orientation, it was about average of the two. The results suggest the different mode of dislocation nucleation, requiring high energy for stacking faults and relatively low energy for partial dislocations. The fitted k were 0.24, 0.30, and 0.27 in the $\langle 100\rangle$, $\langle 110\rangle$, and $\langle 111\rangle$ orientations, respectively. These were different from those of the same diameter of 5 nm with velocity of about 670 m/sec which were not shown here. This result also suggests the anisotropy due to velocity differences.

To study the dislocation nucleation, the centrosymmetry parameter is used which is defined as follows [10]:

$$P = \sum_{i=1,6} |\mathbf{R}_i + \mathbf{R}_{i+6}|^2, \qquad (2)$$

where $\mathbf{R}_i$ and $\mathbf{R}_{i+6}$ are the vectors or bonds corresponding to the six pairs of opposite nearest neighbors in the fcc lattice. The 12 nearest-neighbor vectors for each

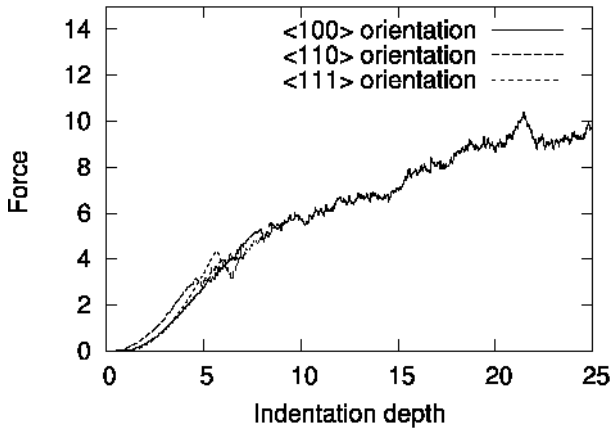

Figure 3: Indentation force vs displacement curves in the three orientation directions. The indenter velocity is about 67 m/sec and its diameter is 5.0 nm. See Fig. 1 caption for units.

atom are first determined in an undistorted bulk fcc lattice with the orientation of the slab. The analogous set of 12 vectors for each atom in the distorted lattice $\mathbf{R}_i$ is then generated by finding those neighbors in the distorted lattice with vectors closest in distance to the undistorted nearest-neighbor vectors. It is possible that this set will contain duplicates or non-nearest neighbors if a given atom has fewer than 12 nearest neighbors or a very distorted local environment. Each "equal and opposite" pair of vectors is added together, then the sum of the squares of the six resulting vectors is calculated. This final number is a measure of the departure from centrosymmetry in the immediate vicinity of any given atom and is used to determine if the atom is near a defect [10].

The centrosymmetry parameter, P is useful to distinguish partial dislocations and stacking faults [10]. The range of values from 0.5 to 4.0 represents partial dislocations and the range between 4.0 and the value of the surface atoms is defined as stacking faults [10]. It is zero for atoms in a perfect nickel crystal lattice, 24.78 $\AA^2$ for surface atoms in the $\langle 100 \rangle$ orientation, 30.88 $\AA^2$ and 6.11 $\AA^2$ for surface atoms in the $\langle 110 \rangle$ orientation, 18.59 $\AA^2$ for surface atoms in the $\langle 111 \rangle$ orientation. Note that the $\langle 110 \rangle$ orientation has two different surface atom values because two layers of surface atoms have different numbers of neighbors. These values assume that the nickel nearest neighbor distance does not change in the vicinity of the defects.

Figure 4 shows early dislocation nucleations in three crystal orientations. For the $\langle 100 \rangle$ orientation, dislocation nucleation starts with stacking faults in the (111) plane. This slip plane agreed with that of the shocked fcc single crystal deformation [1]. Table 1 shows the

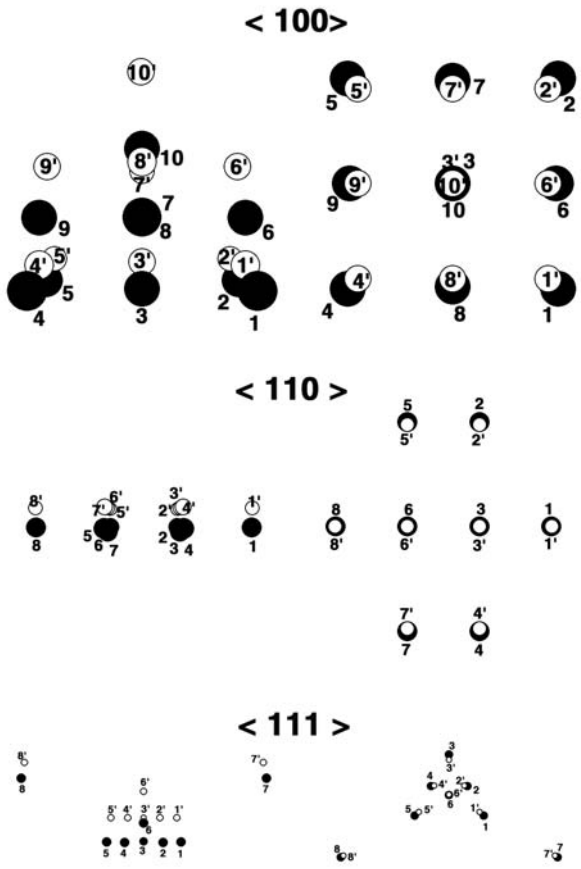

Figure 4: Dislocation nucleations at the time of 28.5, 20.0, 46.0, and at the force of 2.604, 2.363, and 6.734 in Fig. 2 for three crystal orientations, $\langle 100 \rangle$, $\langle 110 \rangle$, and $\langle 111 \rangle$ from top to bottom, respectively. White circles are undistorted atoms and black circles are corresponding distorted atoms. The indenter is moving with constant velocity from top to bottom in the vertical direction (z-axis). Left-handed column shows the active view similar to the plane normal to x-axis and right-handed column is the top view. 10, 8, and 8 atoms are involved in the deformation for $\langle 100 \rangle$, $\langle 110 \rangle$, and $\langle 111 \rangle$ orientations, respectively. Atoms with P>0.5 are selected. The atomic number and its P value are in the Table 1. Prime number is the corresponding undistorted atom number. The atom size in the picture is proportional to the deformed area in the crystal. The centrosymmetry parameter is useful to discriminate different deformation modes, but it fails to provide information on the Burgers vectors of dislocations. Burgers vectors are not shown clearly in the picture.

Table 1: The centrosymmetry, P values at the dislocation nucleation in three crystal orientations. The atom number corresponds to that in Fig. 4.

Atom #	⟨100⟩	⟨110⟩	⟨111⟩
1	4.81	0.82	0.57
2	4.81	0.63	0.55
3	5.32	0.67	0.95
4	4.81	0.63	0.55
5	4.81	0.63	0.57
6	4.75	0.67	0.72
7	4.75	0.63	0.51
8	4.75	0.82	0.51
9	5.75		
10	14.00		

centrosymmetry values for all atoms in Fig. 4. These results suggest that the dislocations propagated non-symmetrically, and they evolved into the mixed modes with stacking faults and partial dislocations. For ⟨110⟩ direction, dislocation nucleation started early at the smallest displacement and propagated through in the mode of only partial dislocations. This slip direction agreed with that of the shocked fcc single crystal deformation [1]. For ⟨111⟩ orientation, the initiation of the dislocation nucleation took the longest time among the three orientations and propagated through with mixed modes of partial dislocations and stacking faults. The centrosymmetry parameter is useful to discriminate the modes of deformation but does not provide helpful information on the Burgers vectors of dislocations. The slip vector defined in the other paper [11] is known to be useful for calculating Burgers vectors of dislocations. It is now under investigation.

4 CONCLUSIONS

I have studied molecular dynamics nanoindentation simulations at surfaces for nickel single crystals with a system size of about 400 000 atoms and with Voter's tabular form of EAM potential. To simulate the elastic-plastic deformation during indentation on a *passivated* surface, a hard-sphere like indenter described by a strong repulsive potential interacted with the fcc metal surface. Anisotropy parameters at the surfaces were investigated as a function of indenter size and indenter velocity for three crystal orientations: ⟨100⟩, ⟨110⟩, and ⟨111⟩. In general, the load-displacement curves followed the Hertzian solution for elastic deformation which is a simple power law of $F = k\ d^{1.5}$ for all orientations, sizes, and velocities of the indenter. However, the indentation curves showed somewhat complicated dependence on the indenter velocity as well as indenter size in the three crystal orientations. These dependencies were quantified by the micro-modulus, k.

In summary, discrete yield phenomena were different in different orientations. Thus, the results showed the dependency of anisotropic elastic-plastic deformation on indenter size, speed and crystal orientations. The centrosymmetry parameter discriminated the mode of deformation. For ⟨100⟩ orientation, dislocation nucleation starts at the mode of stacking faults in the two (111) surfaces. However, the dislocation propagation occurred non-symmetrically and soon evolved into the mixed modes of stacking faults and partial dislocations. For ⟨110⟩ direction, dislocation nucleation occurred in the mode of partial dislocation. For ⟨111⟩ orientation, the dislocation nucleation took the longest time among the three orientations and started at the mode of partial dislocation. However, the geometry was different from that of ⟨110⟩ direction. In this orientation, two dislocation modes, partial dislocations and stacking faults, occurred immediately and almost simultaneously. The results for slip plane and its direction agreed with those observed in the shocked nickel single crystals simulations.

ACKNOWLEDGMENTS

Arthur F. Voter is thanked for the kindness of giving his package of EAM potential models for fcc metals and their alloys. Ethan Ballard is thanked for his proof reading.

REFERENCES

[1] Oyeon Kum, J. Appl. Phys., 93, 3239, 2003.
[2] Oyeon Kum, Nanotech2003, 2, 538, 2003.
[3] S.G. Corcoran, R.J. Colton, E.T. Lilleodden, and W.W. Gerberich, Phys. Rev. B, 55, R16057, 1997.
[4] A. Gouldstone, H.J. Koh, K.Y. Zeng, A.E. Giannakopoulous, and S. Suresh, Acta. mater., 42, 2277, 2000.
[5] A.F. Voter, Los Alamos Unclassified Technical Report #LA-UR93-3901, 1993.
[6] J. Belak, D.B. Boercker, and I.F. Stowers, MRS Bull., 18, 55, 1993.
[7] D.W. Brenner, S.B. Sinnott, J.A. Harrison, and O.A. Shenderova, Nanotechnology, 7, 161, 1996.
[8] R. Pérez, M.C. Payne, and A.D. Simpson, Phys. Rev. Lett., 75, 4748, 1995.
[9] P. Tangyunyong, R.C. Thomas, J.E. Houston, T.A. Michalske, R.M. Crooks, and A.J. Howard, Phys. Rev. Lett., 71, 3319, 1993.
[10] C.L. Kelchner, S.J. Plimpton, and J.C. Hamilton, Phys. Rev. B, 58, 11085, 1998.
[11] J.A. Zimmerman, C.L. Kelchner, P.A. Klein, J.C. Hamilton, and S.M. Foiles, Phys. Rev. Lett., 87, 165507-1, 2001.